Main channel width effects on overtopping-induced non-cohesive fluvial dike breaching

Vincent Schmitz, Ismail Rifai, Lydia Kheloui, Sebastien Erpicum, Pierre Archambeau, Damien Violeau, Michel Pirotton, Kamal El Kadi Abderrezzak & Benjamin Dewals

View supplementary material ↗

Published online: 15 Sep 2023.

Submit your article to this journal ↗

View related articles ↗

View Crossmark data ↗

Research paper

Main channel width effects on overtopping-induced non-cohesive fluvial dike breaching

VINCENT SCHMITZ ⬤ (IAHR Member), *PhD Candidate, Research Group of Hydraulics in Environmental & Civil Engineering, Urban & Environmental Engineering, University of Liège, Liège, Belgium*
Email: v.schmitz@uliege.be (author for correspondence)

ISMAIL RIFAI, Expert Scientist, *Hydro-Québec, Montréal, Canada*
Email: rifai.ismail@hydroquebec.com

LYDIA KHELOUI, Expert Scientist, *National Laboratory for Hydraulics and Environment, Research & Development Division, Electricité de France, Chatou, France*
Email: lydia-externe.kheloui@edf.fr

SEBASTIEN ERPICUM (IAHR Member), *Research Associate, Research Group of Hydraulics in Environmental & Civil Engineering, Urban & Environmental Engineering, University of Liège, Liège, Belgium*
Email: S.Erpicum@uliege.be

PIERRE ARCHAMBEAU, Research Associate, *Research Group of Hydraulics in Environmental & Civil Engineering, Urban & Environmental Engineering, University of Liège, Liège, Belgium*
Email: Pierre.Archambeau@uliege.be

DAMIEN VIOLEAU, Senior Scientist, *National Laboratory for Hydraulics and Environment, Research & Development Division, Electricité de France, and Saint-Venant Laboratory for Hydraulics, Chatou, France*
Email: Damien.Violeau@edf.fr

MICHEL PIROTTON, Full Professor, *Research Group of Hydraulics in Environmental & Civil Engineering, Urban & Environmental Engineering, University of Liège, Liège, Belgium*
Email: Michel.Pirotton@uliege.be

KAMAL EL KADI ABDERREZZAK (IAHR Member), *Expert Scientist, National Laboratory for Hydraulics and Environment, Research & Development Division, Electricité de France, and Saint-Venant Laboratory for Hydraulics, Chatou, France*
Email: kamal.El-kadi-Abderrezzak@edf.fr

BENJAMIN DEWALS (IAHR Member), *Professor, Research Group of Hydraulics in Environmental & Civil Engineering, Urban & Environmental Engineering, University of Liège, Liège, Belgium*
Email: B.Dewals@uliege.be

ABSTRACT
Laboratory experiments were conducted on the breaching of homogeneous non-cohesive sandy fluvial dikes induced by flow overtopping. Tests were conducted using a main channel, an erodible lateral dike and a floodplain. The main channel width and Froude number prior to overtopping were systematically varied. Breach discharge was deduced from water level measurements and mass conservation. High-resolution 3D reconstructions of the evolving breach geometry were obtained using a non-intrusive laser profilometry technique. The main channel width and Froude number show significant influence on the breach expansion and hydrograph. Breach hydrographs are divided into three types, depending on the Froude number and

a non-dimensional main channel width. An adapted fluvial dike breaching model based on the concept of "effective breach width" is proposed. Using the laboratory data, the computed breach discharge is found extremely satisfactory, although the breach downstream expansion is not accurately reproduced by the model.

Keywords: Breach; channel width; fluvial dike; laboratory experiment; non-cohesive; numerical model; overtopping flow

1 Introduction

Failure of fluvial dikes (i.e. levees) induced by overtopping flows can lead to devastating floods, causing significant loss of lives and damage to infrastructure and environment (Di Baldassare et al., 2015; Ward et al., 2017). Accurate prediction of the breach expansion and outflow discharge is crucial to achieve a sound assessment of the inundation risk and to design appropriate countermeasures (ASCE/EWRI Task Committee on Dam/Levee Breaching, 2011; LaRocque et al., 2013; Onda et al., 2019). A comprehensive understanding of dike breaching processes and how various factors (e.g. soil, hydraulic loading conditions, dike geometry, overtopping duration) affect the breach expansion is therefore required. In the following, we focus on non-cohesive homogeneous fluvial dikes.

Dike breaching has received renewed attention in recent years, as evidenced by the increasing number of experimental research studies (see review by Rifai et al. (2017) and Schmitz et al. (2021)). Along with the non-symmetrical expansion of the breach in fluvial dike, the complexity of the breach problem is attributed to the multiplicity of involved physical processes, such as surface erosion and side sloping, among others (Powledge et al., 1989; Schmocker et al., 2014). Available experimental works have attempted to clarify the role of some parameters on the breach expansion, including main channel inflow and downstream boundary condition (Michelazzo et al., 2018; Rifai et al., 2017), floodplain backwater (i.e. presence of water in the floodplain or leveed area prior to dike breaching) (Rifai et al., 2018), grain size of the dike material (Islam, 2012; Kakinuma et al., 2013; Rifai et al., 2021), fine sediment inducing apparent cohesion in the dike material (Rifai et al., 2021), and dike cross-sectional shape (Schmitz et al., 2021). However, other factors still require investigation, such as the main channel width.

To our knowledge, no experimental works were conducted on the effect of channel size for fluvial dike breaching. This issue is of particular interest as the channel size may influence the water level evolution following the breaching. In narrower channels, water level responds rapidly to changes in the boundary conditions, in comparison to wider channels, which are characterized by a greater inertia in water level evolution. This effect interacts directly with the breach flow and, therefore, the breach expansion dynamics. On the other hand, the channel size influences the flow velocity in the near field of the breach with subsequent effects on the breach evolution.

The first aspect, i.e. water level response, was addressed for dam breaching. Wallner (2014) performed laboratory experiments on overtopping induced spatial breaching of dams under different reservoir total volume and shape conditions. Results showed that large storage volumes induce larger breach hydrographs and, for the same storage volume but different reservoir shapes, the highest peak breach discharges were observed for nonlinear reservoir characteristics, e.g. a V-shaped reservoir induces a higher peak breach discharge than a rectangular shaped reservoir with the same storage capacity. These results were confirmed experimentally by Frank (2016). Different reservoir sizes were tested by a real-time adaptation of the reservoir inflow discharge to water level measurements. Results showed that larger reservoir water volumes lead to larger breach hydrographs. Two tests with equal initial storage surface area, but of different reservoir shapes (rectangular *vs* V-shaped), were compared. With the same surface area, the V-shaped reservoir had smaller overall storage volume. The same peak discharge was observed for both tests and differences between the breach hydrographs appeared only past the peak occurrence. Froehlich (2008) related the final average width of an embankment trapezoidal breach as a function of the reservoir volume at the time of failure. Larger reservoir volumes induced wider breaches and longer breach formation times. Using a dataset of 74 cases, Froehlich (2008) showed that reservoir volume was at the forefront of parameters intervening in the breaching process.

The second aspect, i.e. flow velocity field, was briefly analysed by Charrier (2015). Based on water surface velocity measurements, he defined a partition channel width that separates the flow deviated in the breach from that remaining in the main channel. Charrier (2015) showed that for identical breach width, the higher the channel inflow discharge the smaller the partition width and, for the same inflow discharge, the partition width increased with the breach width. Charrier (2015) assumed that no alteration of the velocity field is induced if the partition width is smaller than the channel width, so that the breach discharge is expected to be the same for wider channels.

The present work is part of an ongoing experimental research program on the breaching of non-cohesive sandy fluvial dikes due to flow overtopping. The main objective of this paper is to assess the effects of main channel width on the breach expansion and discharge. Laboratory observations include time series of water levels in the main channel, time series of flow discharges in the main channel and across the breach, and high-resolution 3D reconstructions of the evolving dike geometry by the laser profilometry technique (LPT). The paper is organized as follows: in Section 2, a description of the experimental set-up, measurements, and test program is provided. General results are presented in Section 3 and discussed in Section 4. Conclusions are drawn in Section 5.
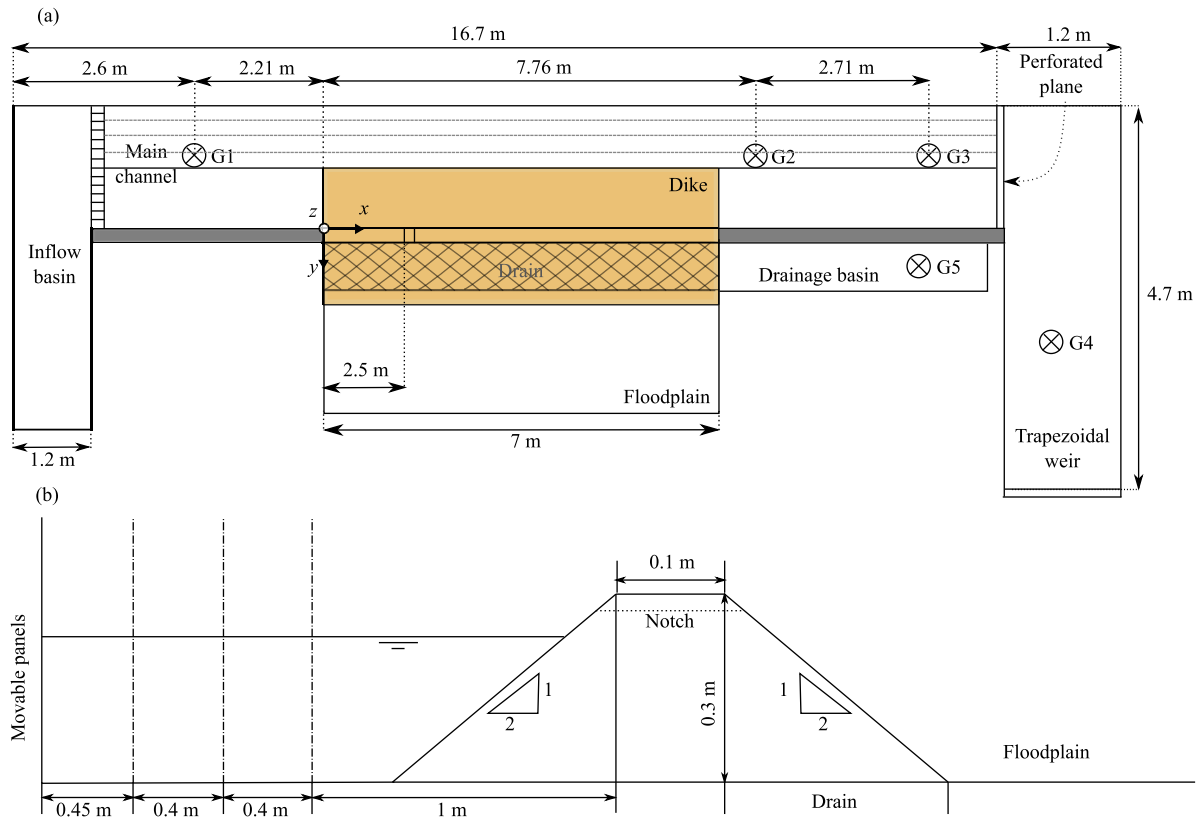
Figure 1   Experimental set-up: (a) plane view; (b) dike cross-section, highlighting modular channel width

2   Laboratory experiments

2.1   *Laboratory set-up*

The experiments were conducted at the National Laboratory of Hydraulics and Environment of the Research and Development (R&D) division of Electricité de France (EDF) using the same experimental set-up as Rifai et al. (2019) (Fig. 1a). The experimental set-up consisted of a 16.9 m long horizontal, straight main channel of trapezoidal cross-section. Its bed width, w_{mc}, could be varied using movable lateral wooden panels, as depicted in Fig. 1b. In this work, four channel widths were considered: 1, 1.4, 1.8 and 2.25 m. A 7 m long trapezoidal dike was built along the right side of the main channel toward a 1×7 m floodplain. The dike material was uniform non-cohesive sand of median diameter $d_{50} = 1$ mm. The dike height, h_d, and crest width, L_k, were set at 0.3 m and 0.1 m, respectively, while both side slopes were fixed to 1:2 (V:H). The main channel and floodplain were at the same level and covered with an impermeable whitewash coating to ensure roughness continuity between the flume, floodplain and dike (Rifai et al., 2017). A drainage system was placed under the dike to prevent seepage flow. As shown in Fig. 1a, a honeycomb straightener was placed upstream of the main channel. A perforated plane was used as regulating weir at the downstream end of the main channel to control water level. Holes were evenly distributed to favour a quasi-uniform velocity distribution over the cross

section. Downstream from the perforated plane, a reservoir collected the outflow discharge. Prior to each test, a 2 cm deep and 10 cm wide notch was dug at the dike crest, 2.5 m from its upstream end, to trigger breaching at this specific location.

2.2   *Test program and test procedure*

Table 1 presents the overall experimental program with the tested inflow discharges, Q_{in}, and the corresponding inlet initial Froude numbers computed before overtopping, which is written:

$$F = \frac{Q_{in}}{A_h\sqrt{gA_h/w_{mc}}} \tag{1}$$

with A_h the flow cross section and w_{mc} the main channel width. Four different channel widths were considered, with varied inflow discharge. In several previous studies (Rifai et al., 2018; Schmitz et al., 2023), the dike height, h_d, was used as a reference for normalizing geometric quantities. Hence, here also we used h_d as a scaling parameter to define a non-dimensional channel width, which can be interpreted as an aspect ratio of the main channel cross section. In total, 10 configurations were tested. Repeatability and reliability of measurements were verified by performing two or three identical experiments for the selected configurations (i.e. configurations C2, D1 and D2).

For each test, the perforated plane was calibrated so that the water level in the main channel, z_w, reached the dike height

Table 1   Test program. Configurations ID ending with 1, 2 and 3 correspond to lower, intermediate and higher Froude numbers, respectively

Conf. ID	Test ID from Rifai et al. (2019)	w_{mc} (m)	Q_{in} (10^{-3} m^3 s^{-1})	w_{mc}/h_d	F
A2	32	1	48	3.33	0.153
B1	33		54		0.108
B2	34	1.4	74	4.67	0.147
B3	35		92		0.184
C1	36		72		0.102
C2	37/38	1.8	98/99	6	0.139/0.140
C3	39		125		0.177
D1	40/41		98/101		0.105/0.108
D2	42/43/44	2.25	139/140/141	7.5	0.149/0.150/0.151
D3	45		160		0.171

for the design inflow discharge. Overtopping started at the initial notch location. Breach discharge was freely released from the floodplain without any storage change nor tailwater effects. Tests were stopped when the breach downstream side closely approached the concrete part of the side opening.

2.3   *Measurements*

Ultrasonic sensors continuously measured the water level (accuracy of ± 1 mm) at three locations in the main channel (G1, G2 and G3), in the outflow tank (G4), and in the drainage tank (G5). An electromagnetic flowmeter measured the inflow discharge, Q_{in} (accuracy of ± 4%). The outflow discharge (accuracy of ± 3.5% of Q_{in}) and drainage discharges were deduced via water level variation at G4 and G5, respectively. The breach discharge, Q_b, was determined from mass balance in the main channel (Rifai et al., 2017). The uncertainty affecting the computed breach discharge may be appreciated by comparing breach discharge estimates in repeated tests. Considering the repetitions of Tests D1, C2 and D2 (Fig. 2), it could be estimated that the uncertainty affecting the breach discharge is of the order of 2% of the inflow discharge on average, while never exceeding 8%. For more details on the monitoring of water levels and flow discharges, readers may refer to Rifai et al. (2018, 2019, 2021).

The 3D breach evolution was monitored continuously by a non-intrusive profilometry technique consisting of a sweeping laser plan (Rifai et al., 2021). Using a digital camera set on a full HD resolution (1920 × 1080 pixels), the recording was performed at 60 frames per second. The 3D reconstruction algorithm of the dike geometry includes optical distortion and refraction correction modules for submerged dike portions. Further details on the breach geometry reconstruction are given in Rifai et al. (2020).

3   Results

The evolution of the ratio of the breach discharge to the inflow discharge, Q_b/Q_{in}, is presented in Fig. 2a for the first 1000 s of each experiment. Figure 2b shows the time-evolution of

the breach extremities location at the crest level. The water level in the main channel is displayed in Fig. S1 in the online supplemental data.

3.1   *Overall breaching dynamics*

The breaching process in non-cohesive homogeneous fluvial dikes can be categorized into three stages (Michelazzo et al., 2018; Rifai et al., 2017):

- Stage 0: Overtopping starts at the initial notch and breaching initiates. The breach expands relatively slowly due to low overtopping flow depth and velocity.
- Stage 1: As the overtopping flow depth and velocity increase, erosion intensifies. Both breach deepening and widening are promoted with a shift of the breach centreline toward the channel downstream end. The breach sides encounter repeated sudden collapses. The breach discharge and the water level in the main channel increases and decreases sharply, respectively.
- Stage 2: The water level in the main channel and the breach discharge tend to stabilize. Breach stops deepening while keeping on widening in the downstream direction only, at a slower pace. The expansion is controlled by side slope failures.

In the following analyses, Stage 0 has been systematically discarded due to the overwhelming influence of the initial notch characteristics during this stage.

Both Stages 1 and 2 are clearly visible in Fig. 2 for all tests. The non-dimensional breach discharge sharply increases for all curves during Stage 1 and tends to stabilize during Stage 2 (Fig. 2a). Similarly, the breach widens quickly during Stage 1 in both upstream and downstream directions (faster toward downstream) while deepening until reaching the main channel bottom (Fig. 2b). During Stage 2, the breach expands only toward downstream at a quasi-constant, slower pace. In general, the transition between both stages becomes more distinct for narrower channels and low Froude numbers, e.g. configurations B1 and C1.
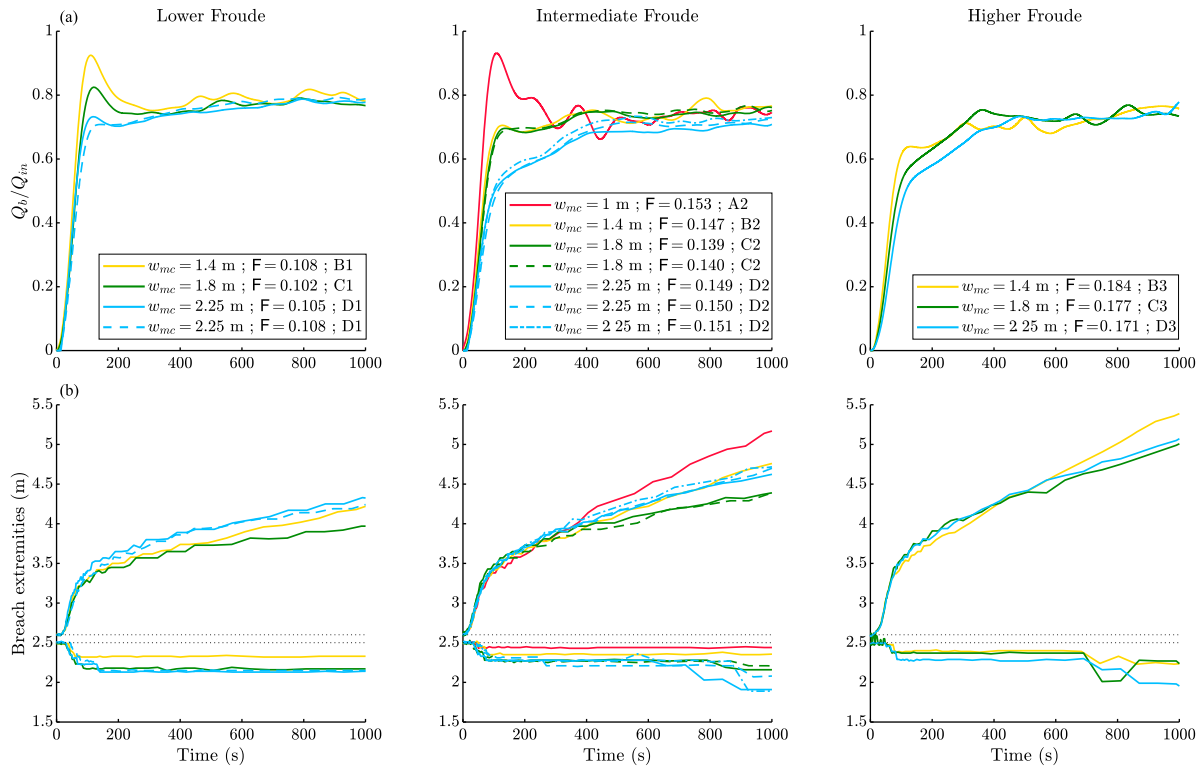
Figure 2 (a) Non-dimensional breach discharge and (b) location of breach extremities (at crest level, along centreline), with initial notch extremities located at 2.5 m and 2.6 m from the dike upstream extremity (dotted lines)

3.2 Influence of main channel width during Stage 1

Results show that part of the hydrographs exhibits a global maximum (Fig. 2a), which gets more distinct when the initial Froude number in the main channel is low and the main channel is narrow. Conversely, it completely fades out for larger Froude numbers and channel widths. Indeed, with a wider channel and for a given breach width, a larger fraction of the main channel flow is not deviated toward the breach, leading to a smaller non-dimensional breach discharge (Charrier, 2015). Another interesting feature is the initial increase rate in the breach discharge that rises when considering a smaller main channel width. This trend is magnified when the Froude number in the main channel is larger.

During Stage 1, erosion is particularly intense, and the dike widens and deepens sharply (Fig. 2b). In all experiments, the downstream widening is significantly larger than the upstream expansion. Though, upstream erosion intensifies when the Froude number in the main channel is reduced. Conversely, the downstream erosion rate rises with the Froude number. This is consistent with earlier observations by Rifai et al. (2017); who showed a substantial increase in the angle between the main channel axis and the breach flow main direction when the Froude number was increased from 0.066 to 0.166. For higher Froude numbers, the flow follows a sharper curve to enter the breach (Charrier, 2015; Rifai et al., 2017). Hence, the load applied by the flow on the downstream breach extremity to modify its direction is higher. For a larger inlet Froude number and

flow momentum along the main channel, the velocity component normal to the main channel axis becomes smaller close to the upstream breach extremity. Consequently, the erosion intensity is more limited in this area. This leads to a gradual shift of the breach centreline towards the channel downstream end as the initial Froude number is increased.

Enlarging the main channel width also influences the breaching dynamics. For similar Froude numbers, increasing the main channel width leads to stronger erosion on the breach upstream extremity. The beginning of Stage 1 corresponds to a sudden breach expansion and release of water volume from the main channel into the floodplain. When the main channel is larger, the water level decreases slightly more slowly due to the greater water volume stored in the channel (Fig. S1). Additionally, the breach mean depth, i.e. ratio between breach area and breach width at crest level, evolves in the same way in all tests during Stage 1 (Fig. S2). A larger water volume in the main channel leads to an increased difference between the main channel water level and the breach bottom. This induces a greater breach discharge, which fosters breach upstream erosion process.

3.3 Influence of main channel width during Stage 2

During Stage 2, the breach discharge in all cases tends to a quasi-stabilized value (around 80% of the inflow discharge), which is hardly affected by the main channel initial Froude

number (Fig. 2a). This is in good agreement with conclusions drawn by Schmitz et al. (2021).

Here, we additionally highlight the relatively low influence of the main channel width on the breach discharge during Stage 2. During this period, breach deepening almost completely ceases, as shown in Fig. S2. With the increase in breach width, erosion on the breach upstream extremity stops as well (Fig. 2b). However, erosion resumes around 800 s for intermediate and high Froude numbers. This phenomenon appears due to the large velocity in the main channel induced by a decrease in the water level (Fig. S1), i.e. flow section, whilst the inflow discharge is kept constant.

The resulting Froude number in the main channel is significantly increased, which favours erosion in this area. After some time, this lateral erosion reaches the dike centreline and becomes visible in Fig. 2b.

The velocity of the flow impacting the breach downstream extremity grows with the Froude number in the main channel. This induces more pronounced breach erosion and downstream expansion. Varying the main channel width has a non-monotonic impact on the breach downstream expansion rate. To understand this feature, two phenomena should be considered (Fig. 3). On one hand, the quasi-stabilized non-dimensional breach discharge is similar in all tests (Fig. 2a) meaning that, for a given Froude number, the breach discharge, Q_b, increases with the main channel width. For a given breach width, the breach discharge is thus larger, so is the flow velocity through the breach, U_b. This increases erosion intensity and breach expansion rate. On the other hand, when the channel width is reduced, the volume stored in the channel decreases and the water level drops more quickly, as shown in Fig. S1. For a given Froude number, the resulting flow velocity in the main channel, U_{mc}, is significantly increased, leading to a stronger impinging jet on the breach downstream extremity (Charrier, 2015; Rifai et al., 2017).

However, the relative weight of each phenomenon depends on the Froude number in the main channel. For low Froude numbers, Fig. 2b shows that erosion is maximum for the widest channel ($w_{mc} = 2.25\,\text{m}$, test D1). By contrast, the narrowest channel induces the strongest erosion rate when the Froude number is large ($w_{mc} = 1.4\,\text{m}$, test B3). This suggests that increasing the Froude number favours the contribution of the second erosion phenomenon listed above.

4   Discussion

4.1   *Classification of hydrographs*

Three main hydrograph types emerged, as illustrated in Fig. 4. The first type (Type A) presents a global maximum during Stage 1, referring to tests B1, C1 and A2. The second type (Type B) exhibits a local maximum discharge at the end of Stage 1. Experiments D1, B2 and C2 correspond to Type B. All remaining tests belong to Type C, in which no maximum is
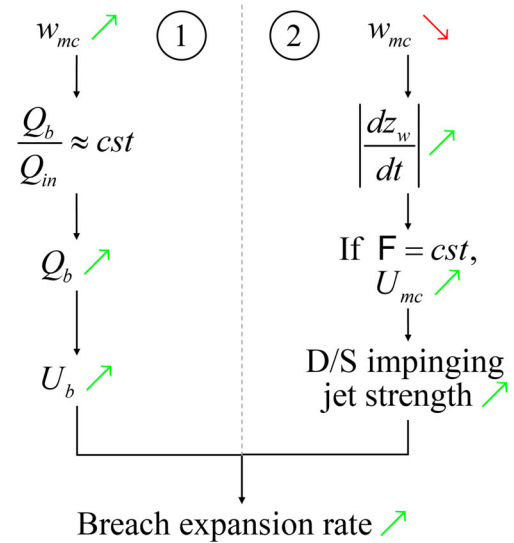

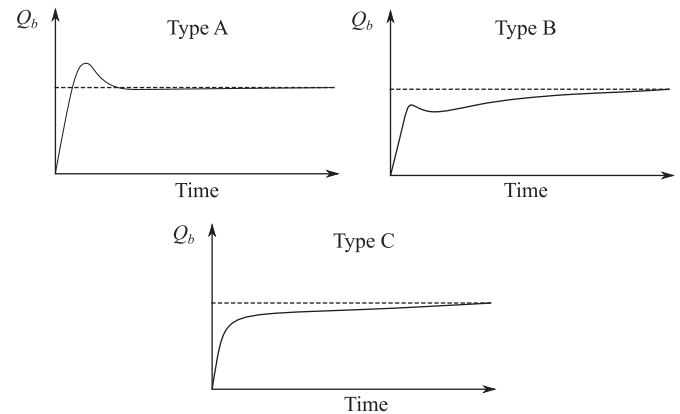Figure 3   Summary of the impact of variations in the main channel width on the breach expansion rate

Figure 4   Three main breach hydrograph types (A, B and C)

observed during Stage 1. During Stage 2, all hydrographs tend to a quasi-equilibrium value, irrespectively of their type.

These three types of hydrographs (A, B and C) were spotted by Schmitz et al. (2021) who suggested that the hydrodynamic process related to fluvial dike failure can be described as a combination of an embankment dam failure, i.e. a sudden water release from a reservoir, and the water flow in a straight open-channel system. Type A hydrographs correspond to a situation where the reservoir feature is prevalent. Conversely, Type C hydrographs are more akin to an open-channel system. Type B lies in-between.

Figure 5 summarizes the partitioning of hydrograph types according to the initial Froude number and the non-dimensional main channel width, w_{mc}/h_d. Eleven experiments led by Rifai et al. (2017), two by Michelazzo et al. (2018) and one by Elalfy et al. (2018) are presented along with tests performed within the present study. It appears that an increase in the Froude number leads to the disappearance of the hydrograph maximum, i.e. transition from Type A to Type C, which agrees with observations by Schmitz et al. (2021). The same trend appears when
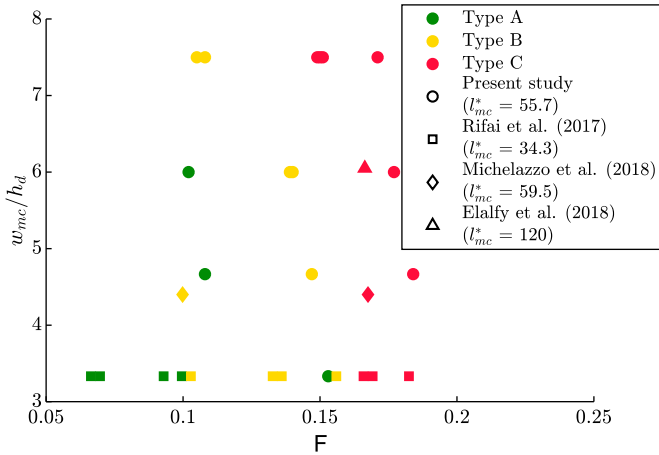
Figure 5   Partitioning of hydrograph types according to initial Froude number in main channel and non-dimensional main channel width. The non-dimensional main channel length $l^*_{mc} = l_{mc}/h_d$ is provided for each test campaign

the non-dimensional channel width is enlarged, but to a much smaller extent. Nonetheless, no clear-cut regions related to specific hydrograph types can be identified, especially for small non-dimensional channel width. This suggests that other parameters affect the hydrograph topology, as for example the drainage system (as highlighted by Michelazzo et al., 2018) or the water volume stored in the main channel. The channel length, l_{mc}, used in this study is about twice that used by Rifai et al. (2017). For a given channel width, it corresponds to an increase of about 50% in the volume stored in the main channel. After breaching, the water level in the main channel drops more slowly when the stored volume is larger, leading to a greater breach discharge during Stage 1. When $F \approx 0.15$ and $w_{mc}/h_d = 3.33$ (Test A2), the hydrograph exhibits an absolute peak discharge during Stage 1 while only a local maximum appears in the corresponding test led by Rifai et al. (2017). In full-scale dike breaching events, the ratio between the main channel width and length is much larger than in laboratory experiments, suggesting that all hydrograph types might not be encountered in practice. However, experimental tests are still extremely useful to validate physically based numerical models, which aim at reproducing physical behaviour of the breaching process regardless of test scale. This is the goal of the following section.

4.2   *Numerical modelling*

The influence of the main channel width on the breach discharge and expansion results from a complex combination of physical phenomena. Here, we adapted an existing semi-analytical physically based dam breaching model to the case of fluvial dike breaching. Our aim is to explore whether the model can capture the influence of the main channel width on the dike breaching dynamics.

The original model is DLBreach developed by Wu (2013), which is composed of three coupled modules: a hydrodynamic

module, a sediment transport module, and a dike morphodynamic module. A flow chart of the numerical model is provided in Figs S4, S5 and S6, while Table S1 describes each involved parameter. The flow is assumed uniformly distributed through the entire trapezoidal breach and the breach expansion is symmetric. However, in fluvial configurations, the flow inertia in main channel direction plays an important role in the breaching process. Laboratory experiments (Fig. S3) and detailed 2D computation (Charrier, 2015) show that the flow through the breach is not uniformly distributed along the breach width, but rather concentrated in the most downstream part of the breach. This phenomenon induces a greater water velocity near the downstream breach extremity (Charrier, 2015), which leads to more intense erosion at this location. Conversely, limited erosion appears on the upstream extremity, leading to largely non-symmetrical breach expansion in the case of fluvial dikes.

In our modified implementation of the model of Wu (2013), we introduced the concept of "effective breach width" to describe the fraction of the total breach width that is effectively used to convey water. During Stage 1, flow velocity fields along both breach extremities tend to be similar due to the small breach width, which leads to a rather symmetrical breach expansion. Consequently, we kept the initial breach expansion description proposed by Wu (2013) until the breach bottom reached the channel bottom. Then, asymmetrical breach widening was enforced by considering an effective breach width equal to $b_{eff\,\%} = 50\%$ of the total breach width, which seemed in line with experimental observations (Fig. S3). This leads to higher flow velocity for a similar breach discharge, so that:

$$U_b = \frac{Q_b}{A_{h,eff}} \qquad (2)$$

with $A_{h,eff} = f(b_{eff\,\%})$ the effective breach flow section. Erosion was computed based on this increased velocity and the related effective breach area. Erosion only appeared on the downstream breach extremity and breach expansion speeded up in that direction. No backwater effect is considered in our model.

Figure 6a compares hydrographs obtained experimentally and numerically using the modified model. Fig. S7a provides a similar comparison using the original dam breaching model (Wu, 2013). Comparisons of the position of the breach extremities are provided in Fig. 6b for the dike breaching model and in Fig. S7b for the original dam breaching model, while Fig. S8 compares the water levels predicted by both numerical models. Overall, results are greatly improved with the dike breaching model, especially for the breach hydrograph. The breach expands toward downstream slightly more quickly with the Froude number, which is consistent with experimental data. However, the new model fails to qualitatively reproduce the non-monotonic influence of the channel width on the breach expansion, i.e. enlarging the channel width always leads to a reduction of the breach widening rate during Stage 2. As mentioned in Section 3.3, this non-monotonic behaviour results from
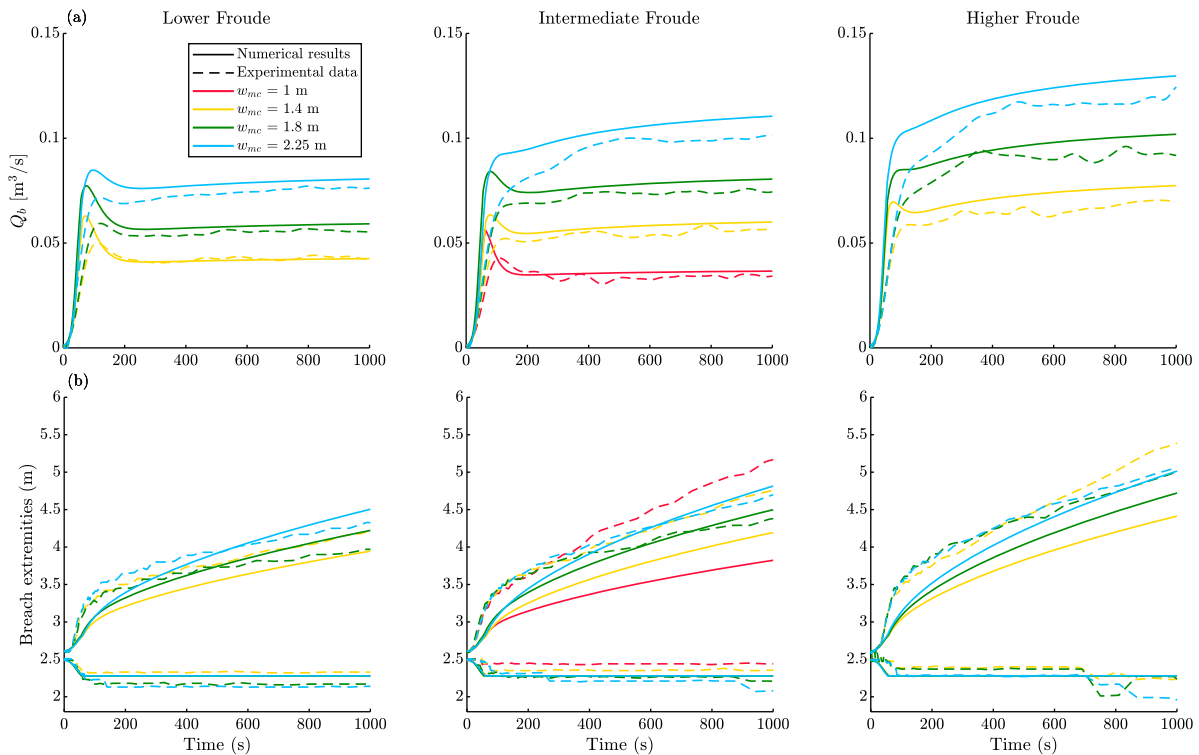
Figure 6   Comparison between results obtained experimentally and numerically with the dike breaching model, i.e. adapted model: (a) breach hydrographs; (b) position of the breach extremities

the competition between two processes, namely the water volume stored in the main channel and the impinging jet on the breach downstream extremity. The adapted numerical model captures the former aspect while being unable to represent the latter. The intensity of the impinging jet on the breach downstream extremity is expected to rise with a decreasing channel width. Our adapted model currently considers the flow through the breach to be parallel to the breach extremities, which is not consistent with this observation. The insufficient breach expansion rate toward downstream during Stage 1 may also be attributed to this phenomenon.

In addition, the experimentally observed breach width is affected by substantial uncertainties because the actual breach geometry is complex and, for the sake of clarity, only the experimentally breach width at the crest level is reflected in Figs 2b and 6b. This cannot reflect all the breach geometric features which influence the flow.

5   Conclusions

This paper highlighted the influence of the main channel width on the breach discharge and expansion in a homogeneous and non-cohesive fluvial dike. Laboratory experiments were conducted, while varying systematically the main channel width and inlet Froude number prior to overtopping. Results showed that the breach hydrograph shape and the breach expansion dynamics highly depend on the main channel inlet Froude number and width. During Stage 1, the initial increase in the breach

discharge became more gradual and no maximum was reached when the Froude number was increased. Enlarging the main channel has a similar effect as increasing the Froude number, i.e. smoother initial increase in breach discharge and disappearance of the maximum at the end of Stage 1. This influence got particularly pronounced for low Froude numbers. However, neither the Froude number nor the channel width significantly impacted the quasi-stabilized breach discharge value during Stage 2. Note that other test features may still influence this value, such as the downstream boundary condition (Rifai et al., 2017) or the main channel bed erodibility (Michelazzo et al., 2018).

During Stage 1, the breach quickly deepened and widened, mainly in the downstream direction. Increasing the Froude number and reducing the main channel width reduced the upstream erosion while having almost no influence on the breach downstream expansion. During Stage 2, both breach deepening and upstream widening stopped. The breach expanded toward downstream at a relatively constant pace, which increased with rising Froude number. The relation between the channel width and the breach erosion rate appeared to be non-monotonic, though of limited amplitude. It is expected to be driven by the combination of two physical phenomena related to the amount of water stored in the main channel on one hand, and the velocity of water impacting the downstream extremity of the breach on the other hand. Their relative weight determined the breach expansion rate.

Hydrographs were categorized in three types, according to the classification proposed by Schmitz et al. (2021). Their partitioning according to the Froude number in the main channel

and the non-dimensional channel width highlighted that Type A hydrographs mostly appear with low Froude number and narrow channels whilst Type C hydrographs emerged with larger Froude numbers and channel widths. Type B hydrographs were obtained for intermediate configurations. However, no clear-cut limits between type zones could be identified. Additional parameters should thus be considered to fully describe this classification.

A semi-analytical physically based fluvial dike breaching model corresponding to an adapted version of the model proposed by Wu (2013) was introduced and its capabilities were assessed using the presented experimental data. The main model improvement consisted in the introduction of the concept of "effective breach width", which lumps the effect of non-uniform flow distribution through the breach. The accuracy of numerical results was significantly improved. However, the new model failed to capture the non-monotonic relation between the channel width and the breach downstream erosion rate during Stage 2.

A wider range of main channel widths should be tested to better understand the impact on the breaching dynamics. Also, the influence of other parameters should be investigated systematically, e.g. dike material properties, drainage system, channel bottom erodibility, but also scale effect. Indeed, larger water volumes are expected to be stored in real world river channel, leading to much slower water level decrease. This would particularly affect flow dynamics and breach expansion during Stage 2. Finally, a way of improving the predictive capabilities of the model presented in this paper would be to include the impact of the impinging jet on the breach downstream extremity, which is expected to boost erosion rate at this location.

Disclosure statement

No potential conflict of interest was reported by the author(s).

Funding

Supplemental data

Supplemental data can be accessed from the online version of the paper. All experimental data are available from the following Zenodo depository: https://doi.org/10.5281/zenodo.1477843.

Notation

A_h = flow cross section (m^2)

$A_{h,eff}$ = effective breach flow section (m^2)
$b_{eff\%}$ = ratio between the effective and total breach widths (–)
d_{50} = median diameter of material (m)
F = Froude number in the main channel prior to overtopping (–)
g = gravity acceleration (m s^{-2})
h_d = dike height (m)
L_k = dike crest width (m)
l_{mc} = main channel length (m)
l_{mc}^* = non-dimensional main channel length (–)
Q_b = breach discharge (m^3 s^{-1})
Q_{in} = inflow discharge (m^3 s^{-1})
t = time (s)
U_b = flow speed through the breach (m s^{-1})
U_{mc} = flow speed in the main channel (m s^{-1})
w_{mc} = main channel bed width (m)
z_w = water level in the main channel (m)

ORCID

Vincent Schmitz http://orcid.org/0000-0003-4442-6487

References

ASCE/EWRI Task Committee on Dam/Levee Breaching. (2011). Earthen embankment breaching. *Journal of Hydraulic Engineering*, *137*(12), 1549–1564. doi:10.1061/(ASCE)HY.1943-7900.0000498

Charrier, G. (2015). *Etude expérimentale des ruptures de digues fluviales par surverse* [Doctoral dissertation]. University of Aix-Marseille. (In French). https://www.theses.fr/2015AIXM4714

Di Baldassare, G., Viglione, A., Carr, G., Kuil, L., Yan, K., Brandimarte, L., & Blöschl, G. (2015). Debates-perspectives on socio-hydrology: Capturing feedbacks between physical and social processes. *Water Resources Research*, *51*(6), 4770–4781. doi:10.1002/2014WR016416

Elalfy, E., Tabrizi, A. A., & Chaudhry, M. H. (2018). Numerical and experimental modeling of levee breach including slumping failure of breach sides. *Journal of Hydraulic Engineering*, *144*(2), 04017066. doi:10.1061/(ASCE)HY.1943-7900.0001406

Frank, P.-J. (2016). *Hydraulics of spatial dike breach* [Doctoral dissertation]. ETH Zürich, Switzerland. https://www.research-collection.ethz.ch/bitstream/handle/20.500.11850/128470/1/eth-50528-01.pdf

Froehlich, D. C. (2008). Embankment Dam Breach Parameters and their Uncertainties. *Journal of Hydraulic Engineering*, *134*(12), 1708–1721. doi:10.1061/(ASCE)0733-9429(2008)134:12(1708)

Islam, S. (2012). *Study on levee breach and successive disasters in low-land through numerical and experimental approaches* [Doctoral dissertation]. Nagoya University,

Japan. https://nagoya.repo.nii.ac.jp/record/15319/file_preview/k9879.pdf

Kakinuma, T., Tobita, D., Yokoyama, H., & Takeda, A. (2013). Levee breach observation at Chiyoda experimental flume. In S. Fukuoaka, H. Nakagawa, T. Sumi, & H. Zhang (Eds.), *ISRS 2013. Proceedings of the 12th International Symposium on River Sedimentation* (pp. 1013–1020). CRS press.

LaRocque, L. A., Elkholy, M., Hanif Chaudhry, M., & Imran, J. (2013). Experiments on urban flooding caused by a levee breach. *Journal of Hydraulic Engineering*, *139*(9), 960–973. doi:10.1061/(ASCE)HY.1943-7900.0000754

Michelazzo, G., Oumeraci, H., & Paris, E. (2018). New hypothesis for the final equilibrium stage of a river levee breach due to overflow. *Water Resources Research*, *54*(7), 4277–4293. doi:10.1029/2017WR021378

Onda, S., Hosoda, T., Jaćimović, N. M., & Kimura, I. (2019). Numerical modelling of simultaneous overtopping and seepage flows with application to dike breaching. *Journal of Hydraulic Research*, *57*(1), 13–25. doi:10.1080/00221686.2018.1442882

Powledge, G. R., Ralston, D. C., Miller, P., Chen, Y. H., Clopper, P. E., & Temple, D. M. (1989). Mechanics of Overflow Erosion on Embankments. II: Hydraulic and Design Considerations. *Journal of Hydraulic Engineering*, *115*(8), 1056–1075. doi:10.1061/(ASCE)0733-9429(1989)115:8(1056)

Rifai, I., El kadi Abderrezzak, K., Erpicum, S., Archambeau, P., Violeau, D., Pirotton, M., & Dewals, B. (2018). Floodplain backwater effect on overtopping induced fluvial dike failure. *Water Resources Research*, *54*(11), 9060–9073. doi:10.1029/2017WR022492

Rifai, I., El Kadi Abderrezzak, K., Erpicum, S., Archambeau, P., Violeau, D., Pirotton, M., & Dewals, B. (2019). Flow and detailed 3D morphodynamic data from laboratory experiments of fluvial dike breaching. *Scientific Data*, *6*(1), 53. doi:10.1038/s41597-019-0057-y

Rifai, I., El Kadi Abderrezzak, K., Hager, W. H., Erpicum, S., Archambeau, P., Violeau, D., Pirotton, M., & Dewals, B. (2021). Apparent cohesion effects on overtopping induced fluvial dike breaching. *Journal of Hydraulic Research*, *59*(1), 75–87. doi:10.1080/00221686.2020.1714760

Rifai, I., Erpicum, S., Archambeau, P., Violeau, D., Pirotton, M., El Kadi Abderrezzak, K., & Dewals, B. (2017). Overtopping induced failure of noncohesive, homogeneous fluvial dikes. *Water Resources Research*, *53*(4), 3373–3386. doi:10.1002/2016WR020053

Rifai, I., Schmitz, V., Erpicum, S., Archambeau, P., Violeau, D., Pirotton, M., Dewals, B., & El Kadi Abderrezzak, K. (2020). Continuous Monitoring of Fluvial Dike Breaching by a Laser Profilometry Technique. *Water Resources Research*, doi:10.1029/2019WR026941

Schmitz, V., Arnst, M., El Kadi Abderrezzak, K., Pirotton, M., Erpicum, S., Archambeau, P., & Dewals, B. (2023). Global sensitivity analysis of a dam breaching model: To which extent is parameter sensitivity case-dependent? *Water Resources Research*, e2022WR033894. doi:10.1029/2022WR033894

Schmitz, V., Erpicum, S., El Kadi Abderrezzak, K., Rifai, I., Archambeau, P., Pirotton, M., & Dewals, B. (2021). Overtopping-Induced Failure of Non–Cohesive Homogeneous Fluvial Dikes: Effect of Dike Geometry on Breach Discharge and Widening. *Water Resources Research*, *57*(7), e2021WR029660. doi:10.1029/2021WR029660

Schmocker, L., Frank, P.-J., & Hager, W. H. (2014). Overtopping dike-breach: Effect of grain size distribution. *Journal of Hydraulic Research*, *52*(4), 559–564. doi:10.1080/00221686.2013.878403

Wallner, S. (2014). *Influence of reservoir Shape and Size on The Flood Wave Caused by Progressive Overtopping Dam Failure* [Doctoral dissertation]. TU Wien. doi:10.34726/hss.2014.25148

Ward, P. J., Jongman, B., Aerts, J. C., Bates, P. D., Botzen, W. J., Loaiza, A. D., ... Winsemius, H. C. (2017). A global framework for future costs and benefits of river-flood protection in urban areas. *Nature climate change*, *7*(9), 642–646. doi:10.1038/nclimate3350

Wu, W. (2013). Simplified physically based model of earthen embankment breaching. *Journal of Hydraulic Engineering*, *139*(8), 837–851. doi:10.1061/(ASCE)HY.1943-7900.0000741